Infrared Physics and Technology, Volume 89, March 2018, Pages 231-241
DOI:10.1016/j.infrared.2018.01.011

Sodium sulfate crystallisation monitoring using IR Thermography

P. Vazquez *[1] , C. Thomachot-Schneider [1], K. Mouhoubi [2], J-L. Bodnar [2], N. P. Avdelidis [3,4], D. Charles [1], D. Benavente [5]

* *Corresponding Author*

[1] *GEGENAA EA 3795, University of Reims Champagne-Ardenne (URCA), 2 esplanade Roland Garros, 51100 Reims, France*

[2] *CATHERM, GRESPI EA 4694, University of Reims Champagne-Ardenne (URCA), Moulin de la Housse BP 1039, 51687 Reims, France*

[3] *Department of Electrical and Computer Engineering, Université Laval, G1V 0A6, Quebec City (Quebec), Canada*

[4] *Aerospace Integration Research Centre (AIRC), College Road, Cranfield, MK43 0AL, UK*

[5] *Dpto. Ciencias de la Tierra y del Medio Ambiente, Universidad de Alicante, 03080 Alicante, Spain*

Abstract

In this work, the evaporation of sodium sulfate droplets with different concentrations and at different temperatures were studied using infrared thermography (IRT). IRT allows to detect the evaporation evolution, the crystal growth and for the first time, to observe in vivo the heat release related to sodium sulfate crystallisation. A detailed study revealed that dendritic Thenardite III crystals appeared at the edge of all the crystallised droplets, though they showed a fast increase of temperature related to crystallisation only when a hydrated phase crystallised also from the droplet. The observation of the heat of crystallisation is thus directly related to the supersaturation of the droplet and consequently to temperature. In addition, IRT detection is circumscribed by the location of crystallisation. The heat can be observed and measured only when the crystallisation occurs in the interface solution – air.

Keywords: sodium sulfate; infrared thermography, crystallisation, heat release, supersaturation

1. Introduction

The crystallisation of sodium sulfate generates a wide interest in different fields. The main issue is the damage produced in porous materials, with special concern in stone buildings of cultural heritage [1]. The crystallisation pressure causes the fracturation of the pores and consequently the deterioration of the stone [2]; [3]; [4]. In addition, the field of energy storage benefits from the heat exchange during the phase transition [5]; [6]. Fundamental researches focus on this salt because of its complexity and the need for a better understanding of its crystallisation [7]; [8].

In nature, sodium sulfate appears commonly in two forms. The first is Thenardite V (anhydrous phase) which crystallises as efflorescence and produces mainly an aesthetic change on stone surface, without strong mechanical damage [9]; [10]; [11]; [12]. The second is mirabilite (decahydrated phase) which crystallises as subflorescence and produces the most severe damage on the stones [13]; [14]; [15]. Thenardite V and mirabilite are the stable phases of the sodium sulfate system, but also two metastable phases are found in determinate conditions. The first is the anhydrous Thenardite III which appears at room conditions, and the sodium sulfate heptahydrate, which is a metastable phase appearing commonly before mirabilite at low temperatures [16]; [17]; [18]; [19]; [20].

In laboratory studies, sodium sulfate materialises through several stable and metastable phases [21]. The temperature, relative humidity and concentration leading to preferential crystallisation of one phase over another. Differences are noticeable if supersaturation is obtained by solution cooling or by evaporation (e.g. [22]; [23]). In addition, factors such as the nature of the substrate,

contact angle, impurities or air currents may play a determinant role in the crystallisation of a given phase in the evaporating droplet experiments [24]. In addition, different phases can coexist within a droplet, elevating the complexity of the process [13]; [25]. This implies that the variability of the results from an evaporating brine droplet is enormous and the repeatability unknown. As mentioned by Genkinger and Putnis (2007) [22], sodium sulfate behaviour is extremely complex, and contemporary research shed light on some questions but gave rise to new ones.

This complexity has led to the use of new and accurate techniques allowing for a deeper understanding of the different processes. Environmental scanning electron microscopy (ESEM) started being used for the assessment of sodium sulfate crystallisation around year 2000 [11]; [26]. This technique threw light on salt hydration and dehydration as well as on the different phases formed. Neutron Magnetic Resonance (NMR) was introduced in recent years for the research of sodium sulfate heptahydrate crystallisation [17]; [18]. This technique allows to observe in-situ crystallisation by controlling temperature and measuring solution concentration. Thus, the supersaturation occurring at the moment of crystallisation can be recovered. Environmental XRD allows to observe in vivo the phase change and coexistence with variatins in temperature and humidity [27]. Another analytic technique is Raman spectrometry, this allows to determine which phase corresponds to a fixed crystal with accurate results for sodium sulfate heptahydrate in the case of Hamilton and Menzies 2009 [28] and Linnow et al., (2013) [29]. Even more accurate techniques were utilised to study salt crystallisation, like Synchrotron X-ray tomography to observe salt crystallisation within a porous stone [30] or Rainbow Schlieren deflectometry and liquid crystal thermography [31] providing answers about heat release during crystallisation. Numerous models were introduced in order to simulate the real behaviour of different salts and mixtures, related to crystallisation pressure as well as chemical interaction [7]; [8]; [32], [33].

The use of infrared thermography (IRT) has been widely adopted over the last several years in many areas [34]; [35]. It has proven to be an important non-destructive technique for civil engineering works even for those requiring special attention as in the case of cultural heritage [36]; [37]; [38]; [39]; [40]. One of the last applications of this technique was laboratory detection of salts [41]; [42] and also in real artworks [43].

This non invasive and non destructive technique was recently used for the study of compounds crystallisation as in Parsa et al., (2015) [44] who studied CuO droplet evaporations. Vazquez et al., (2015) [45] presented the study by IRT of sodium chloride from an evaporating droplet, with the differentiation of the different phases in relation to thermosignal variation. Some chemical processes triggered heat exchange reactions such as water evaporation (endothermic reaction) or crystallisation (exothermic reaction). In some cases, this heat was not sufficient to be detected by the IRT camera. However, crystallisation from a droplet entailed a variation in shape and thus in emissivity. This variation in emissivity allowed to observe other phenomena of the crystallisation process as a great evaporation before crystallisation or creeping [45]; [46].

The main aim of this research is to deepen the analysis of sodium sulfate crystallisation by means of IRT. This assessment will be obtained by solving three questions

- What is the thermal response of sodium sulfate resulting from evaporating droplets?
- How repeatable are the results in terms of thermal response, crystal habitus and occurring phases?
- Is there a specific crystal phase associated to a specific thermal response?

2. Experimental Setup

2.1 Measurement protocol

In this study, the thermal effect of the crystallisation of sodium sulfate droplets was assessed by means of a FLIR SC655 long wave infrared thermography camera (7.5 –14 μm) with a temperature ranging from -40 to 150° C and an accuracy of ± 2% of the reading. The detector is an uncooled array of microbolometers. Image size is 640 x 480 pixels and the noise signal is approximately 40 mK. The recorded signal is called thermosignal (TS). The TS depends on the temperature and emissivity and is expressed in isothermal units (I.U.). All measurements were conducted using the passive IRT mode. Prior tests concluded that the optimal recording speed (frame rate) was 1 image per second throughout the test for the conditions used. The images were treated and analysed with the ThermaCAM Researcher 2.10 and ResearchID software (FLIR).

The supersaturation needed for sodium sulfate crystallisation was induced by the evaporation of the solvent. The droplets were placed on black adhesive tape (3M), which served as a reference material and was stuck to a glass slide. Its emissivity was determined to be 0.96 in the wavelength analysed by the camera [47]. The 3M tape used as support was cleaned with alcohol before each test to minimise the presence of impurities. Temperature was set constant with a cooling plate Tetech CP-061 that kept it with a precision of 0.01 °C. The droplets were dropped with a micropipette with the same quantity (5 μL) in each case. During the experimental setup the risks associated to environmental variations were minimised such as control of temperature and humidity of the room with 20 ± 2°C and 40 ± 5% RH respectively, none artificial or natural light source that cousl influence the signal and the room temperature and a closed environment with no external interferences. Nevertheless, some variables were introduced due to the manuallity of some tasks such as the deposition of the droplets. For example, preliminary tests revealed that for 20 droplets the contact angle could vary between 22 and 40°.

Once the droplets crystallised, the crystal morphology and distribution were assessed by optical microscopy with the aid of an Olympus SZH-ILLB stereomicroscope with a digital Tri-CDD camera (Sony, DXP 930) and image analysis software from Microvision Instruments.

2.2 Experimental

Nucleation and growth experiments presented a probabilistic behaviour. Thus, experimental conditions were kept the most identical possible with six droplets tested at the same time in one support so that the differences in the crystallisation process were not due to the environmental conditions. The droplets were placed manually with the most similar spacing among them.

Sodium sulfate solutions were prepared with distilled water at 7, 14, 20 and 28% wt concentrations (purity of >99 %, Sigma Aldrich). These concentrations were chosen because 14% wt is the concentration used in natural stone standards for resistance to salt crystallisation (UNE_EN 21370) and 28% is the concentration close to saturation at room temperature. The 20% concentration was chosen as the intermediate value and 7% as a weak concentration in order to evaluate the influence of concentration in the crystallisation. Saturation index, SI, describes the saturation degree of mineral phases. It is defined as:

$$SI=\log(IAP/K) \quad (1)$$

where IAP is the ionic product and K is the equilibrium constant. SI is calculated according to the Benavente et al., (2015) [33].

Lower and intermediate concentrations were tested in order to determine the importance of concentration in the thermal response of the evaporating droplets. In all cases, the solutions were mixed at 50°C and stirred for 1 hour to avoid crystal seeds. This temperature kept the solution far from the saturation threshold and thus it avoided the crystallisation during the droplet

deposit. The six droplets of each concentration evaporated at the same time on the cooling plate at 50, 25, 20 and 15°C respectively.

Additionally to image observation, TS was monitored in several points of the droplet. For a better comprehension, data were treated in relation to the 3M tape as follows (2):

$$\Delta TS = TS_{droplet} - TS_{3M} \quad (2)$$

Negative values corresponded to lower emissivity or/and lower temperature than the black tape. Since the highest emissivity of salt crystals is similar to 3M tape, positive values (higher than TS_{3M}) mean only higher temperatures.

3. Results

When a droplet is placed on a substrate, it evaporates through all its surface. Within the droplet, there is a flow that replenished the edge with the liquid from the centre. When the evaporation is enough to create a supersaturation of the saline solution, small crystals appeared. These crystals are usually concentrated on the edge, due to the higher supersaturation in this area and to the flow of small crystals from the centre to the edge.

3.1 Thermal responses of droplet evaporation

The thermal response of salt solution evaporating from a droplet observed with IRT consists of three phases [45]: (I) homogeneous evaporation, (II) crystal growth driven by evaporation and (III) crystal growth fed by solution creeping. Phases I and II always appear whereas the type of salt and the environmental conditions will condition the occurrence of phase III. These three

phases were defined for NaCl droplets and they may not fit in exactly with the behaviour of other salt types.

Figure 1 shows the TS of the whole process of crystallisation of sodium sulfate at different temperatures, from the deposit of the droplet down to the stabilisation of the signal after crystallisation. The droplet evaporation (Phase I) was measured as a linear increase in ΔTS, i.e. the $TS_{droplet}$ (negative) approaches the TS_{3M} (zero). Sometimes a rapid slope appeared, i.e. the ΔTS reduced drastically (Fig 1, a) that indicated the total evaporation at this point. At 50°C and 25°C evaporation started instantaneously with the deposit of the droplet on the plate. When the temperature was set at 20°C and 15°C, the evaporation did not start until several minutes later and even hours in extreme cases. After a determinate time, there was an inflexion point in which TS started increasing linearly at the same rate approximately as that at 25°C (Fig 1c, d). During this Phase I, crystals could grow within the solution, nevertheless they were not observed by the IRT due to the low crystallisation energy and the heat dissipation into the droplet. The detection limit of the IRT camera was not high enough to register these temperature variations.

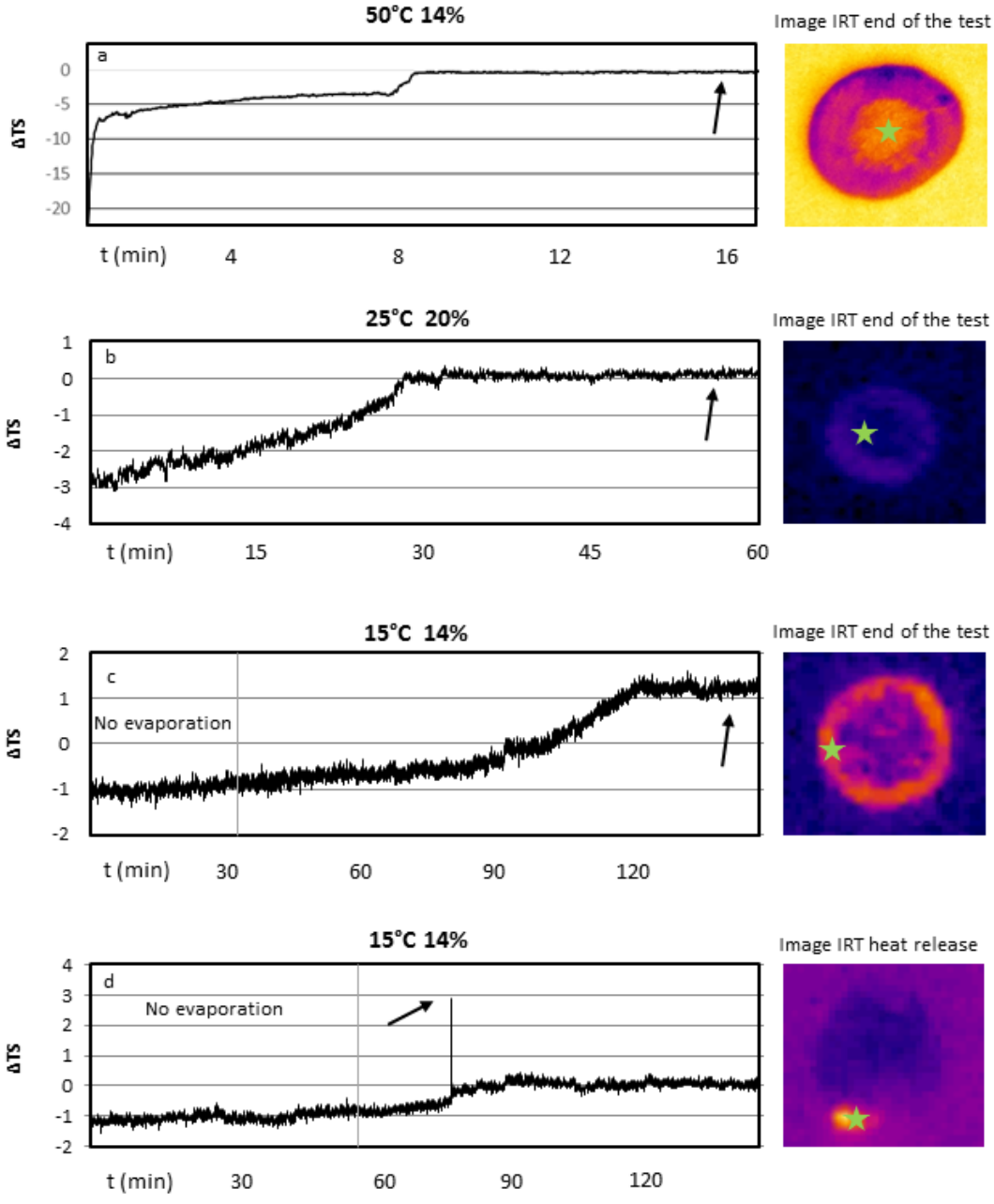
50°C 14%
Image IRT end of the test
a
ΔTS
0
-5
-10
-15
-20
t (min)
4
8
12
16
25°C 20%
Image IRT end of the test
b
ΔTS
1
0
-1
-2
-3
-4
t (min)
15
30
45
60
15°C 14%
Image IRT end of the test
c
No evaporation
ΔTS
2
1
0
-1
-2
t (min)
30
60
90
120
15°C 14%
Image IRT heat release
d
No evaporation
ΔTS
4
3
2
1
0
-1
-2
t (min)
30
60
90
120

200

201

Figure 1

Fig 1: Examples of ∆TS evolution with time of the droplet during crystallisation on the point indicated by a star. The image of the droplet corresponds to the ∆TS indicated by an arrow on the graph. a) Droplet evaporation with no crystal formation in the measuring point; b) Similar process than in a) with different substrate temperature; c) A crystal appeared at the measuring point with positive TS at the end of the crystallisation; d) Heat release due to crystallisation ("flash") observed as a peak of TS increase.

Phase II was characterised by a crystal growth on the edge and in the centre of the droplet. This phase starts at the inflexion point after the homogeneous increasing slope of phase I. At the end of evaporation (Fig 1 a, b c), crystals showed a slightly different TS from the reference black tape due to a low emissivity produced by the shape effect and a difference of temperature between the substrate and the environment (observed also in [45]). The environment temperature was fixed at 22°C so that if the temperature of the support was higher than that of the environment (22°C), the crystals would show colder TS and if temperature of the support was colder than the environment, crystals would appear hotter.

In some points (Fig 1 d), the heat release due to crystallisation was high enough for the observation of some early crystal formation leading to a sudden peak of TS (due to a temperature increase). This peak was called "flash" since it was observed as a photographic flash with the IRT.

Weak creeping was observed in a few cases (Phase III) [45]. As explained in Vazquez et al., (2015) [45], after Phase II, when no solution was visible with the IRT, a series of intermittent decreases of the TS around and on the previously formed crystals were observed. This indicated that evaporation was not yet complete and that stepped crystal growth or dehydration processes

were still occurring. The IRT signal recorded intermittent decrease in the TS and only when this intermittent variation stopped, was crystallisation considered to be completed.

3.2 Types of exothermal reactions

During a sodium sulfate droplet evaporation, in some cases an increase of temperature was recorded with IRT, corresponding to the exothermal reaction linked to crystallisation. This phenomenon called “flash” could reach a few degrees and last for a few seconds. After that, TS returned to the same or slightly higher values. The flash phenomenon started at a single point and moved with a wicking effect through the droplet. Regarding the wick movement, the flash could be divided out into three forms (Fig 2):

- **Single Ring** (Fig 2 top, Figure 3 - Video 1)**:** it could appear before any crystal was visible in the droplet or with several crystallisations in the centre and edge of the droplet. In both cases, the solution was still visible by IRT. In this case, a starting point showed a higher TS than the rest and it started moving through the droplet edge in one direction. This direction could be clockwise or contrarily, without any priority. Once the high TS had completed part of the droplet perimeter, the temperature dropped to that of the solution and evaporation accelerated.
- **Double Ring** (Fig 2 middle): similarly to the first case, a point of the droplet edge increased its temperature. From this point, the heat propagated clockwise or in counter-clockwise directions through the droplet edge until confluence and recovery of solution temperature. The droplet continued evaporating after this process. Sometimes, the movement of the high TS was not continuous but intermittent and the whole loop could be divided into two or three steps.

- **Scanning** (Fig 2 bottom)**:** from the first heating point, the high thermosignal spread linearly across the whole droplet like a scan. Solution remained in some parts of the droplet that continued evaporating.

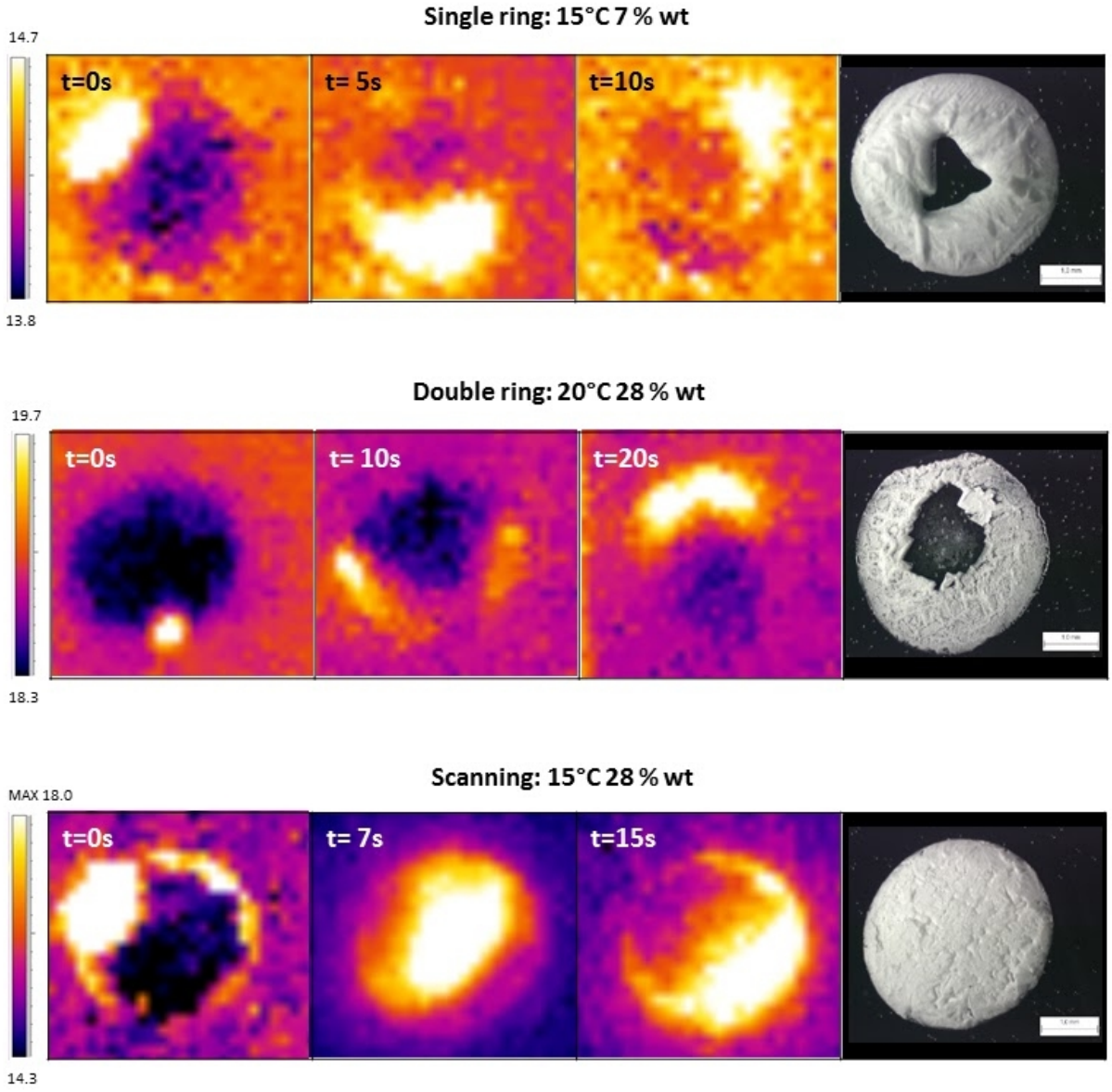

Fig 2: Different steps of flash phenomena and the corresponding crystallised droplet at the end of the evaporation viewed under magnification eye. Top: single ring; Middle: double ring; Bottom:

scanning. The crystallised droplet with white and powdery aspect corresponded to thenardite as product of dehydration of a previous hydrated phase.

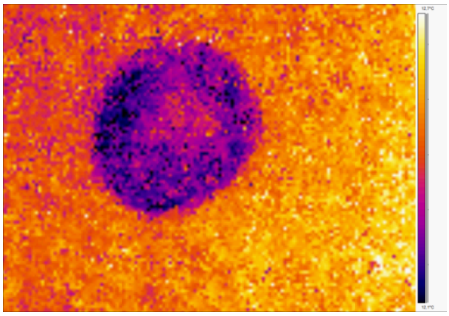

Figure 3 - Video 1: Flash with ring shape recorded in a droplet with 14% concentration at 15°C.

3.3 Relation between thermal response, temperature and saline concentration

For the four different temperatures (50°, 25°, 20°, and 15°C) and the four different concentrations (7, 14, 20, and 28% wt), the results of the thermal response are shown in Table 1.

Table 1: For each temperature and concentration, number of flashes over the 6 droplets tested (sudden TS increases), minimal and maximal ΔTS measured and flash type description.

		7%	14%	20%	28%
50°C	N° Flash	0	0	0	0
	Min-Max ΔTS (I.U.)				
	Shape				
25°C	N° Flash	0	0	0	0
	Min-Max ΔTS (I.U.)				
	Shape				
20°C	N° Flash	1	1	1	4
	Min-Max ΔTS (I.U.)	2	2.2	2.4	2.2-3.6
	Shape	sr	dr	dr	dr, sc
15°C	N° Flash	4	2	2	3
	Min-Max ΔTS (I.U.)	2.2-3.6	3.2-3.6	2.0-2.2	1.2-6.8

Shape	dr, sc	sr	dr	sc, sr

sr: single ring; dr: double ring; sc: scanning.

At 50°C and 25°C no increase in TS was observed for any concentration. Droplets evaporated showing low TS in the whole droplet.

When temperature was set at 20°C, only one of the six droplets tested at the same time exhibited a flash phenomenon. The increment of TS was comparable for all concentrations. Values were found around 2 I.U. The most common type of flash was the ring, single in low concentrations and double in high concentrations.

At 15°C, the flash phenomena became more frequent. For all the concentrations, the number of flashes per droplet was between 2 and 4. In general, values of ΔTS were higher than those at 20°C, reaching even almost 7 I.U. for 28% concentration. The type of flash was variable, with single and double ring, and also scanning at high concentrations (Fig 1, 2).

3.3 Relation between thermal response and crystal shape

The observation with naked eye revealed a difference in the type of crystals in the droplets that exhibited flash or not.

- Droplets that did not show a flash phenomenon showed transparent and elongated crystals.

Two elongated crystal shapes were found in these droplets i) transparent crystals forming aggregates in fan-shape that corresponded to Thernadite (V) [11]; [13] and ii) transparent crystals with dendritic shape that corresponded toThernardite (III). The latter owes its whitish color to small prismatic crystals (Thernadite V) that appeared on the thenardite (III) during the last evaporation process [11]; [13]; [25]; [29]; [30]. Both types of elongated crystals (fan-shape

and dendritic) grew from the edge to the centre. Thenardite (V) is the stable anhydrous phase and Thenardite (III) the metastable anhydrous phase of sodium sulfate. The thickness of this ring-like crystal varied in relation to temperature and concentration. Figure 4 shows that the thickness was lower at low concentrations and low temperatures, increasing linearly with concentration.

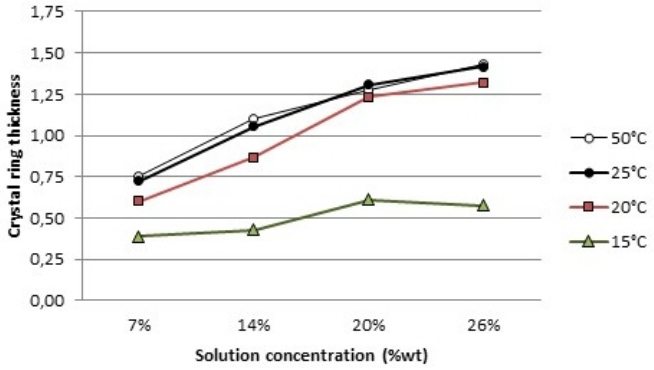

Fig 4: Ring thickness with temperature and concentration.

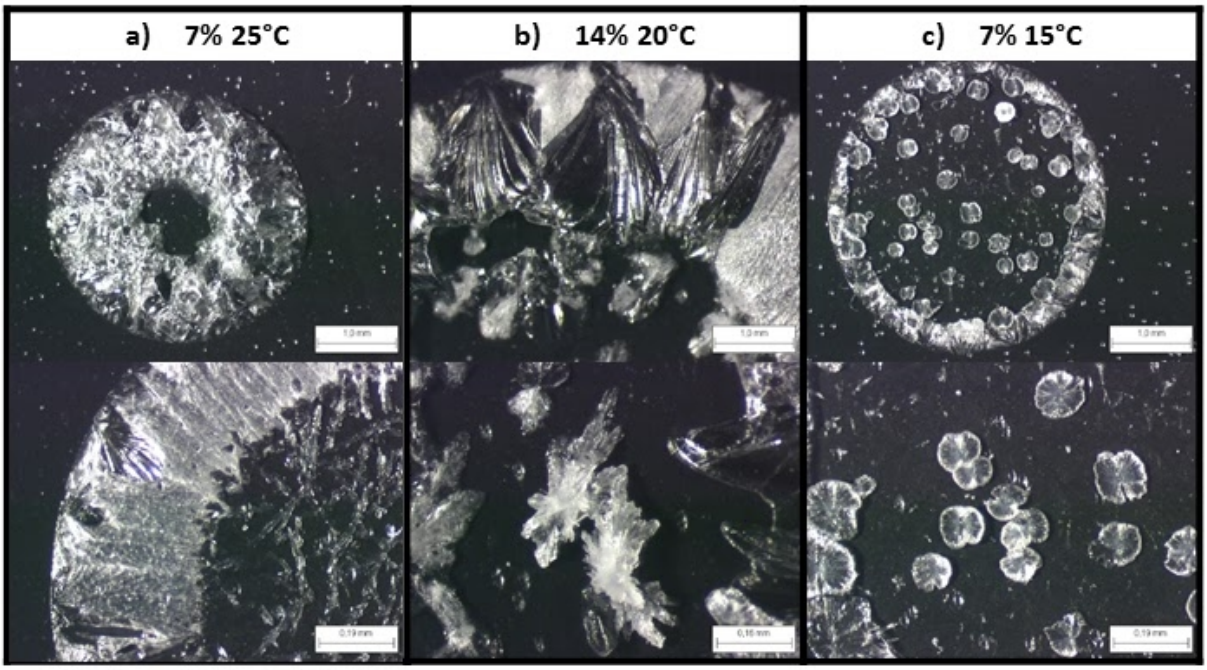

312 Fig 5: Crystal shape of droplets evaporating without flash phenomenon. Thenardite V and
313 Thenardite III are visible in each droplet.
314
315 At 20°C, droplets that did not show a flash, appeared similar to those at 50 and 25°C, with
316 Thenardite V transparent, with radial elongated crystals and Thenardite III from the edge to the
317 droplet centre and, in this case, bigger crystals of Thenardite III in the centre. At 15°C, the
318 droplets that did not experiment a flash showed lot of dogteeth on the edge (Thenardite V) and
319 small radial crystals on the edge and in the droplet centre (Thenardite III).
320 In the case of 7 and 14% concentrations and for all temperatures, all the crystals were ordinated
321 figuring a radial geometry towards the centre of the droplet (Fig 5). These crystals were longer
322 with a 14% concentration and they occupied more than half of the droplet. With 20 and 26%
323 concentrations these crystals were more chaotic in the centre, masking the radial structure
324 converging from the edge. In the centre of the ring, small dendritic crystals appeared dispersed.
325
326 - Crystallised droplets that showed flash phenomena (ring or scanning) were white and
327 powdery which corresponded to a dehydrated phase formed from a previous hydrated phase
328 (Fig. 4).
329 During the tests carried out at 20°C and 15°C, transparent crystals appeared in first place (phase
330 not recognised during the monitoring). However, after total crystallisation the crystals become
331 white and with a powdery aspect, sometimes with geometrical remnants of transparent crystal
332 shapes (Fig 2). This kind of white crystals are typical of stable Thenardite V as a product of
333 dehydration indicating the existence of a previous hydrated phase. The ring flashes (simple and
334 double) originated on the droplet edge and they moved only through the border [25]. Closer
335 observation with the binocular microscope, focusing on the edge crystals where flash flashes
336 originated, showed a different type of crystals from the rest of the droplet. Dendritic transparent

337 of Thenardite III grew among hydrated phases and remained transparent after dehydration,
338 indicating the absence of overgrowth Thenardite V.
339
340 **4. Discussion**
341
342 **4.1 Droplet evaporation**
343
344 Droplets with four concentrations were evaporated at different temperatures ranging from 15°C
345 to 50°C in laboratory conditions (22°C and 33% RH). The water evaporation enthalpy is around
346 40 kJ/mol and the evaporation heat around 2250 kJ/Kg. As evaporation is an endothermal
347 process, the IRT TS is lower in the evaporating area. However, as observed in Vazquez et al.,
348 (2015) [45], the low TS of this process is not related only to the evaporation process. Droplet
349 emissivity depends on the observation angle. For observation angles of 45 or more, the
350 emissivity was found to decrease [48]. As evaporation proceeds, the contact angle is reduced
351 and the droplet surface becomes flatter. This produces a homogeneous increase of the
352 measured emissivity (Fig 2). In addition, during this study the evaporation process showed slight
353 random variations on TS. These fluctuations were too weak and they were measured as TS
354 noise. However, since temperature remains constant, these variations may correspond to the
355 likely convective movements due to concentration gradients at the evaporating surface [22]; [31];
356 [49].
357 The differences of temperature between the substrate and the environment may create various
358 crystallisation patterns due to Marangoni effects. After comparing the results obtained by Parsa
359 et al., (2015) [44] and the results of this research, it can be stated that the differences due to
360 Marangoni effect related to differences in temperature can be neglected. There were more
361 variations between droplets tested at the same time in the same conditions than with droplets
362 tested at different temperatures.

363

364 **4.2 Thermal response of sodium sulfate**

365 *4.2.1 Influence of the crystal location and temperature for the detection of the exothermal*

366 *reaction*

367

368 During phase change (liquid to solid), the temperature of the crystal remains constant.

369 Nevertheless, this process involves a heat exchange with the surroundings that can be

370 sometimes measured by IRT. Two options must be considered: i) the crystallisation occurs inside

371 the droplet as in the case of faceted crystals or ii) the crystallisation occurs at the air-solution

372 interface as in the case of the edge dendritic crystals.

373

374 i) If the crystallisation occurred inside the droplet, the heat released that could be measured by

375 the camera corresponded to the indirect signal of the solution heating.

376 $$TS \Leftrightarrow \xi_s S_d \sigma\left(T_s^4 - T_{env}^{\ 4}\right) + \tau_s \xi_c S_c \sigma\left(T_c^4 - T_{env}^{\ 4}\right) \quad (3)$$

377

378 Where,

379 $\xi_s S_d \sigma\left(T_s^4 - T_{env}^{\ 4}\right)$ *is the indirect emission*

380 $\tau_s \xi_c S_c \sigma\left(T_c^4 - T_{env}^{\ 4}\right)$ *is the direct emission*

381 TS= IRT thermosignal

382 ξ_s = emissivity of the solution

383 ξ_c = emissivity of the salt crystal

384 Sd: proyected droplet surface

385 Sc= proyected crystal surface

386 σ = Stephan Boltzmann constant

387 τ_s = solution transmissivity

388 T_s = temperature of the solution

389 T_c = temperature of the crystal

390 T_{env} = temperature of the environment

391

392 Taking into account the ratio volume crystal/volume droplet, this heating can be considered
393 negligible. The direct transmission from the droplet to the air can also be considered insignificant
394 because of the low transmissivity of the water. During this test, the growth of hydrated or anhydre
395 crystals in the centre of the droplet was observed due to emissivity variations when the solution
396 formed a film around the crystals. However, according to the above mentioned, the heat of
397 crystallisation of crystals in the centre of the droplet was not observed by IRT.

398

399 ii) If the crystallisation occurred at the liquid-air interface**,** two parameters were responsible for
400 the received signal. The heat was released in the droplet edge producing an increase of
401 temperature of the surrounding solution. In this case, the affected volume was much lesser that
402 in case i) and thus this area of the droplet heats up high enough to be detected by the IRT
403 camera. Besides, there is a direct transmission from the crystal to the air that can also be added
404 to the droplet signal.

405 $$TS \Leftrightarrow \xi_s S_d \sigma\left(T_s^4 - T_{env}^4\right) + \tau_a \xi_c S_c \sigma\left(T_c^4 - T_{env}^4\right) \quad (4)$$

406

407 Where

408 τ_a is the air transmissivity

409

410 *4.2.2. Supersaturation and maximum increase of temperature*

411

412 Most of the studies of sodium sulfate thermodynamics were carried out with solutions in closed
413 systems. In these cases, supersaturation leading to crystallisation is obtained by decreasing the
414 temperature. During crystallisation, the heat is released and diffuses through the solution, being
415 measured as an increase of temperature [20]; [23]; [31]; [50]. This temperature increase during
416 crystallisation is directly related to the solution supersaturation. Espinosa et al., (2008) [23]
417 observed an increase of temperature of 0.1°C for a supersaturation ratio of a salt in the solution
418 of 1.8, whereas a supersaturation ratio of 7.5 implicated an increase of 11°C. Vavouraki and
419 Koutsoukos (2012) [50] measured a maximum increase of T of 3.5°C with a relative
420 supersaturation of 0.54 (or a saturation index (SI) of 0.19). Since there is not heat loss into the
421 atmosphere, temperature values in a closed system were expected to be higher than in open
422 system evaporating droplets. Nevertheless, the increase of temperature could be comparable
423 with the results of this IRT study even if a big variation (1.6 -6.8 I.U.) was measured.
424
425 According to the observations with IRT, the highest increase of temperature appeared mainly at
426 the beginning of the crystallisation. This agrees with other studies in closed systems that did not
427 register other signs of heat release even with further crystallisation and its consequent increase
428 of supersaturation [23] or that measured different heat peaks but which corresponded to different
429 crystallisation phases [20].
430 In this study, more than one increase of temperature (flash) in different parts of one droplet and
431 separated in time were observed in isolated cases. These increases were mostly in the form of
432 ring flashes. Egan et al., (2014) [31] found a more important temperature increase during
433 nucleation but also during dendritic crystal growth, which could explain the various flash
434 phenomena observed.
435 The duration of the heat release went from several minutes [50] to more than one hour in closed
436 systems [20]; [23], while the flashes observed in this study with IRT lasted only a few seconds.
437

4.2.3. Thermal behaviour and crystallisation patterns in relation to T:

Figure 6 shows the initial concentrations and temperatures and the increasing concentration pathways during evaporation.

At 50°C, all the solutions were undersaturated, with a saturation index of -1.53 for 7% to -0.73 for 28%, and the increase in concentration due to evaporation should lead to Thenardite crystallisation (Fig 6). Observation of the formed crystals showed that they are solid and transparent to quasi transparent with different shapes but all similar to Thenardite III and Thenardite V [11]; [13]; [25]; [51]. At 50°C temperature, the crystallisation enthalphy is positive for all the solution concentrations even supersaturated [52], explaining the lack of temperature increase during crystallisation. Temperature decrease was neither observed.

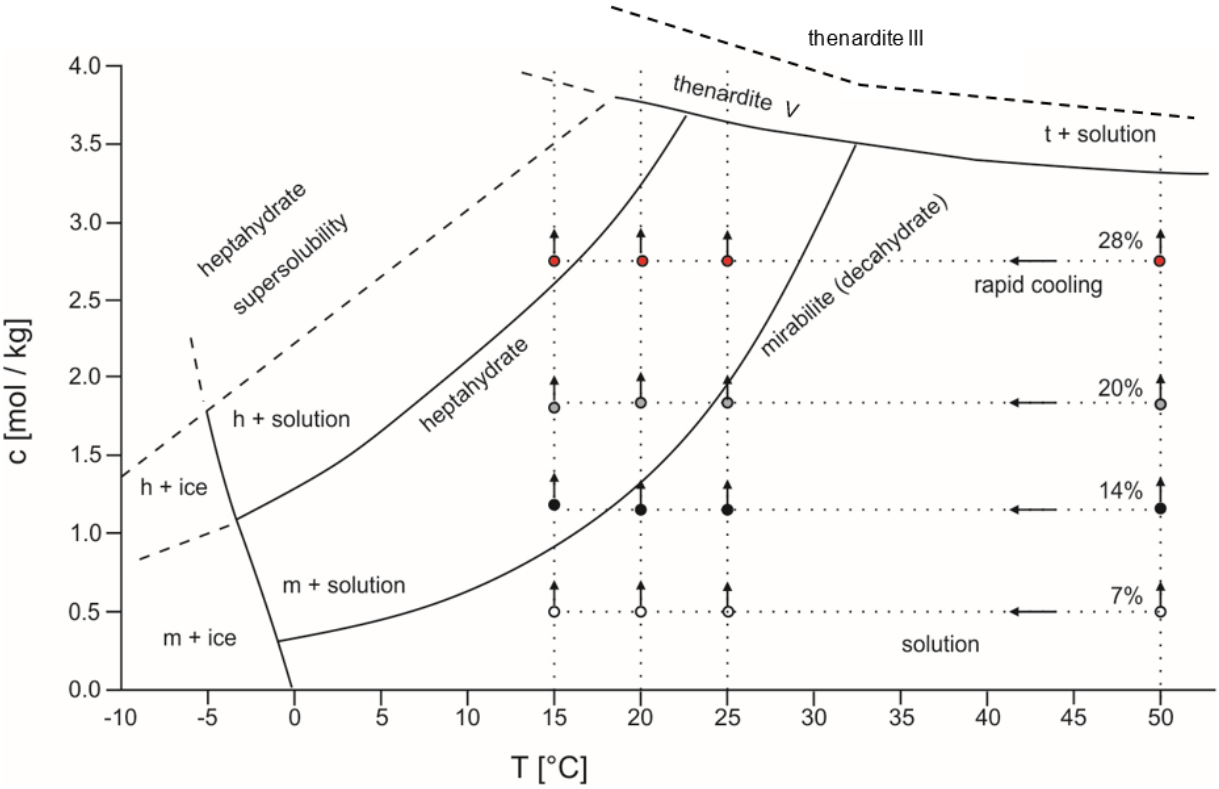

452

453

454 Fig. 6: Initial concentrations and temperatures of the tested droplets. The arrows indicate the
455 fast cooling from the solution at 50°C to the temperature of the test, and the increasing
456 concentration pathways during evaporation.

457

458 At 25°C, the solutions with 7, 14 and 20% concentrations were undersaturated in relation to
459 mirabilite crystallisation (SI are -0.82, -0.32 and -0.03 respectively) meanwhile during the cooling
460 of the 28% concentration the threshold of mirabilite saturation was crossed (SI= 0.17). In spite
461 of these differences, all the droplets crystallised similarly to those at 50°C, with the ring-like
462 shape of acicular Thenardite V and the dendritic crystals of Thenardite III on the droplet edge
463 and isolated dendritic crystals in the centre. During evaporation at 25°C, saturation of the
464 solution aimed at forming mirabilite. However, supersaturation aimed at producing the mirabilite
465 nucleation was not high enough and so it was Thenardite that crystallised [7]. At this

466 temperature, no heat release was recorded with the IRT in spite of having negative enthalpies
467 (exothermal reactions) for supersaurated concentrations. The solubility limit of Thenardite
468 crystals is 35% [25] and due to this fact, the heat released is too weak to be detected by the
469 camera.
470
471 At 20°C the 7 and 14% solutions remained under the mirabilite saturation threshold (-0.6 and -
472 0.1 respectively) whereas the 20 and 28% solutions rapidly cooled down to the solubility
473 boundaries between mirabilite and heptahydrate and then started evaporating. In this case, five
474 of the six droplets followed the same behaviour as the ones at 50°C and 25°C with Thenardite
475 as the predominant crystallisation phase (Phase III and Phase V). However, one of the six
476 droplets for each concentration performed differently. These droplets showed an increase of
477 temperature on the edge during crystallisation, with a single ring flash at 7%, a scanning flash
478 at 14% and a double ring flash at higher concentrations. The crystallisation enthalpy was
479 negative and with a heat release superior than at 25°C [52]. This fact could explain the detection
480 with the IRT camera, although the high supersaturation reached in the nucleation spot, the higher
481 energy released by metastable phases, together with a difference in the crystallised volume
482 could enhance the recorded signal. After the test, these crystals were white and powdery,
483 characteristic of Thenardite V formed by dehydration of hydrated phases [13]. The dehydration
484 is produced by evaporation pulses, observed as dark intermittent signal with IRT [13]; [45]. The
485 hydrated phase that corresponds to these crystals is however not clear. On one hand, some
486 authors crystallised or found mirabilite at temperatures around 20°C. According to Telkes, 1952
487 [5], at 20°C mirabilite precipitated in an spontaneous way if concentration was 3.7m, Vavourakis
488 and Koutsoukos (2012) [50] found mirabilite after introducing mirabilite seeds at 20°C and 18°C
489 and Donkers et al., (2015) [6] crystallised mirabilite at 22°C. On the other hand, in a 7% droplet,
490 a truncated pyramid of four sides appeared within the rest of the crystals, reminding of
491 heptahydrate habit found in Hamilton et al., (2008) [17] (Fig 8) . Even if most of the researches

showed the appearance of heptahydrate at low temperatures [17]; [18]; [19]; [20] others found the heptahydrate at higher temperatures (22°C) [27]; [53]. Higher temperatures allow higher concentrations that can be set for heptahydrate to crystallise [18]. All these data cast doubts about the identification or not of the crystal shown in Fig 7 as heptahydrate at 20°C.

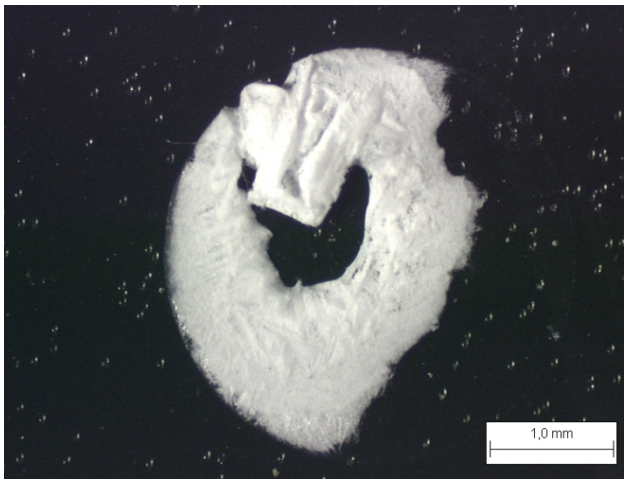

.

Fig 7: Crystal showing a heptahydrate shape (according to Hamilton et al., 2008).

At 15°C the 7% solution started evaporating in undersaturated conditions meanwhile the 14 and 20% crossed the solubility limit of mirabilite (SI are 0.13 and 0.4 respectively) and the 28% crossed the heptahydrate threshold (SI=0.06). In this case, for every concentration, half of the droplets showed crystals with similar acicular and dendritic habits to those recognised as Thenardite V and III. The main difference is that in hotter conditions, crystals grow from the edge to the centre of the droplet with a fan-like shape, and at 15°C most of them grow with a circle-radial shape. This means that even at 15°C and with supersaturated conditions in mirabilite and even heptahydrate, Thenardite has 50% possibilities of crystallising. The other half of the droplets showed flash phenomena, in which the ring flash was more frequent than the scanning. The differences in temperatures measured during the flash (Table 1) revealed that in general the increase was higher at 15°C that at 20°C according to the higher exothermal enthalpy [52] and the increase of supersaturation leading to crystallisation with lower temperatures [53]. The

final crystals were also white and powdery with no well-defined shape. One case was the exception. Fig 8 shows three droplets evaporating at 15°C and with the same 14% concentration. All the three are white and powdery crystals and were produced by dehydration of a hydrated phase. However, Fig 8c shows the crystallised droplet without any flash phenomena. In the two cases in which a ring flash was observed with IRT, the droplets keep their circle shape with a very thin crystal layer (Fig 8 a and b). The flash (sudden increase of temperature) corresponds to the crystallisation of crystals at the edge following a "wicking effect" [54]. However, in the only case of dehydrated crystals that did not show a flash, the crystals grew in the centre of the droplet and nothing remained in the droplet edge. This indicates that the growth of big hydrated crystals is not related to temperature increase.

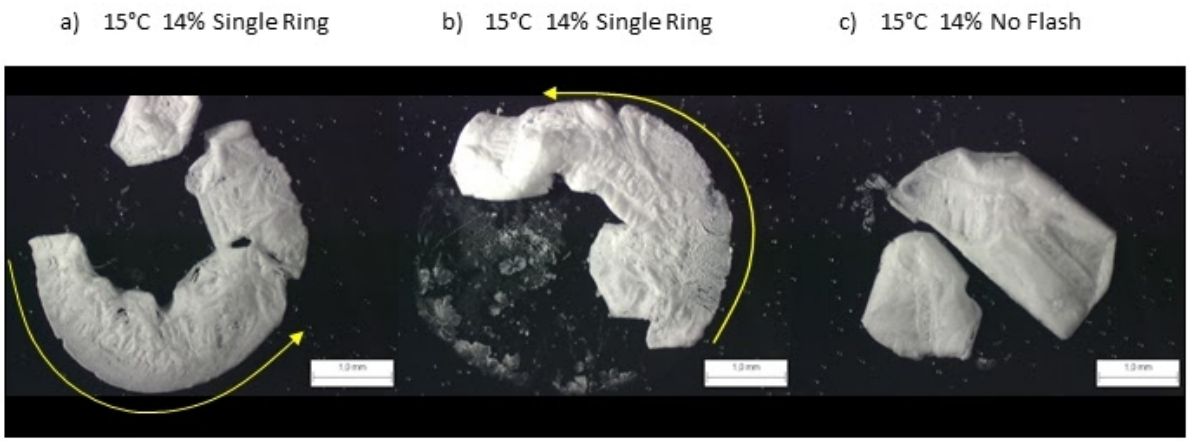

Fig 8: a, b) sodium sulfate crystals that showed ring flash phenomena and the direction of the flash during their crystallisation. c) sodium sulfate crystals of droplets that did not show any flash phenomenon.

4.2.4 Determination of the phase that corresponds to the highest heat release

The droplets were observed with higher magnification in order to determinate which sodium sulfate phase was producing the flash. Strikingly, at first sight, dendritic crystals of Thenardite III were responsible of either behaviours, heat release (flash) and no heat release (no flash). In Fig

530 8c these dendritic crystals are not present. Fig 9 shows in detail the dendritic crystals observed
531 in hydrated and dehydrated crystallisations.
532

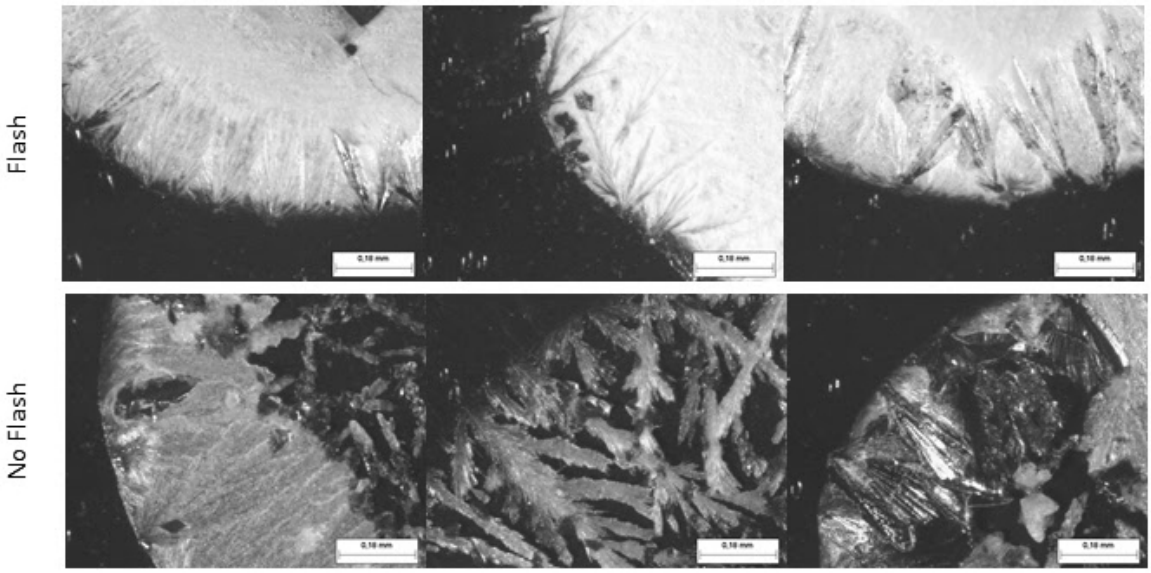

533
534 Fig 9: Detail of crystals that initiated the flash compared to those that did not flash (15°C, 14%
535 concentration).
536
537 The crystallisation of dendritic crystals corresponding to metastable Thenardite III (paragraph
538 3.1) is common in environmental conditions [5]; [16]. Egan et al., (2014) [31] precipitated sodium
539 sulfate at low temperatures and they observed an increase of temperature during nucleation but
540 also during the growth of dendritic crystals. After the dendritic growth, they observed another
541 more faceted phase that grew slowly.
542 Füredi Milhofer et al., (1990) [55] reported that in supersaturated conditions, the solutions with
543 lower supersaturation led to dendrite precipitation while hydrated and compact crystals resulted
544 from higher supersaturations. This explains that at higher temperatures, supersaturations only
545 entailed the crystallisation of Phase III which needed less concentration to nucleate.

In addition, with the decrease of temperature, the nucleation threshold decreases as supersaturation increases. In both cases there is an exothermal reaction, but at 15°C the energy released is higher [52] and thus it is within the detection range of the IRT camera. This explains that for the same crystallisation phase (dendrites of phase III) high supersaturations involve a heat release higher than low supersaturations. In high supersaturations, even with the initial precipitation of phase III, hydrated crystals continued precipitating, confirming the high supersaturation needed for a hydrate to crystallise instead of the anhydrous phase.

5. Conclusions and perspectives

IRT is a promising tool for salt crystallisation studies, which allows differentiating some processes that cannot be distinguished with visual methods. IRT has been successfully applied to the sodium sulfate system and has permitted to characterise the heat released of both stable and metastable phases. In this study, IRT allowed to observe in vivo the heat released during crystallisation and its relation to temperature and supersaturation.

The main pourposes of this research were to determine the thermal response of sodium sulfate resulting from evaporating droplets, and if there is a specific crystal phase associated to a specific thermal response. The main findings were:

- During droplet evaporation, the first crystals that appear are the dendritic Thenardite crystals, which is the metastable phase that arises with the lowest supersaturation degrees. A heat release is produced by these dendritic crystals (Thenardite III) growing on the edge of the droplets that involved an increase of temperature in a precise small spot on the droplet edge that propagates following a wicking effect through this contact.
- At the end of the crystallisation process, a hydrated phase was observed in droplets showing flash (even if the flashes are produced by Thenardite). Due to the fact that crystals are

already present, and if saturation is on the threshold of the mirabilite - heptahydrate, this phase should be to crystallise.

- At lower temperatures, the mineral saturation at the moment of the first crystallisation (dendrites) and crystallisation enthalpy is higher and so is the heat released by this process.
- Thermosignal can only be observed mainly when the crystallisation takes place in the interface droplet air. However, some phenomena such as scanning did not find any explanation.

Other of the goals of this research was to determine the flash phenomena repeatability in terms of thermal response, crystal habitus and occurring phases. Regarding the results from six droplets, further analysis will be needed to state a behaviour and a probabilistic result. Additionally, further clarification is needed regarding some questions that resulted during these research studies e.g. it is necessary to understand why heat release takes the form of scanning; to determine the statistical repeatability of one or the other phases of flash phenomena at temperatures below 20°C; and test the feasibility of IRT in other conditions, at lower temperatures to detect heptahydrate or during hydration/dehydration processes.

Acknowledgements

This work was partially funded by the BQR call from the University of Reims Champagne-Ardenne (project Transels) and the project FLUTE funded by the University of Reims Champagne-Ardenne and the Region Grand-Est (France).

597 **References**

598

599 [1] Winkler, E.M. and Singer, P.C., 1972. “Crystallization pressure of salts in stone and
600 concrete”. Geological society of America bulletin, 83(11), pp.3509-3514.
601 [2] Flatt, R.J. “Salt Damage in Porous Materials: How High Supersaturations Are Generated.”
602 Journal of Crystal Growth 242, no. 3 (2002): 435–454
603 [3] Benavente D, García-del-Cura MA, Fort R, Ordóñez S (2004a) “Durability estimation of
604 porous building stones from pore structure and strength”. Engineering Geology 74:113-
605 127.
606 [4] Angeli, M., Benavente, D., Bigas, J.P., Menéndez, B., Hébert, R. and David, C., 2008.
607 “Modification of the porous network by salt crystallization in experimentally weathered
608 sedimentary stones”. Materials and Structures, 41(6), pp.1091-1108.
609 [5] Telkes, M. “Thermal Energy Storage in Salt Hydrates.” Solar Energy Materials 2, no. 4
610 (1980): 381–393.
611 [6] Donkers, P. A. Linnow, J., K., Pel, L., Steiger, M. and Adan O. C. G. “Na 2 SO 4· 10H 2 O
612 Dehydration in View of Thermal Storage.” Chemical Engineering Science 134 (2015):
613 360–366.
614 [7] Marliacy, P., Solimando, R., Bouroukba, M., and Schuffenecker, L. “Thermodynamics of
615 Crystallization of Sodium Sulfate Decahydrate in H 2 O–NaCl–Na 2 SO 4: Application
616 to Na 2 SO 4· 10H 2 O-Based Latent Heat Storage Materials.” Thermochimica Acta
617 344, no. 1 (2000): 85–94.
618 [8] Steiger, M., Kiekbusch, J. and Nicolai, A. “An Improved Model Incorporating Pitzer’s
619 Equations for Calculation of Thermodynamic Properties of Pore Solutions Implemented
620 into an Efficient Program Code.” Construction and Building Materials 22, no. 8 (2008):
621 1841–1850.
622 [9] Zehnder, K. and Arnold, A., 1989. “Crystal growth in salt efflorescence”. Journal of crystal

growth, 97(2), pp.513-521.

[10] Charola, A.E. and Lewin, S.Z., 1979. “Efflorescences on building stones-SEM in the characterization and elucidation of the mechanisms of formation”. Scanning electron microscopy, 1, pp.378-386.

[11] Rodriguez-Navarro, C., Doehne, E., and Sebastian, E. “How Does Sodium Sulfate Crystallize? Implications for the Decay and Testing of Building Materials.” Cement and Concrete Research 30, no. 10 (2000): 1527–1534.

[12] Vázquez, P., Luque, A., Alonso, F.J. and Grossi, C.M. “Surface Changes on Crystalline Stones due to Salt Crystallisation.” Environmental Earth Sciences 69, no. 4 (2013): 1237–1248.

[13] Rodriguez-Navarro, C., Doehne E. “Salt Weathering: Influence of Evaporation Rate, Supersaturation and Crystallization Pattern.” Earth Surf. Process. Landforms 24 (1999): 191–209.

[14] Tsui, N., Flatt, R.J. and Scherer, G.W., 2003. Crystallization damage by sodium sulfate. *Journal of cultural heritage*, *4*(2), pp.109-115.

[15] Benavente D, García-del-Cura MA, García-Guinea J, Sánchez-Moral S, Ordóñez S (2004b) The role of pore structure in salt crystallization in unsaturated porous stone. Journal of Crystal Growth 260:532-544

[16] Grossi, C. M., Esbert, R. M. Suarez del Rio, L.M., Montoto, M. and Laurenzi-Tabasso, M. “Acoustic Emission Monitoring to Study Sodium Sulfate Crystallization in Monumental Porous Carbonate Stones.” Studies in Conservation 42, no. 2 (1997): 115–125.

[17] Hamilton, A., Hall, C. and Pel, L. “Sodium Sulfate Heptahydrate: Direct Observation of Crystallization in a Porous Material.” Journal of Physics D: Applied Physics 41, no. 21 (2008): 212002.

[18] Derluyn, H., Saidov, T.A., Espinosa-Marzal, R. M. Pel, L., and Scherer G.W. “Sodium Sulfate Heptahydrate I: The Growth of Single Crystals.” Journal of Crystal Growth 329,

649 no. 1 (2011): 44–51.
650 [19] Saidov, T. A., Espinosa-Marzal, R.M. Pel, L. and George W. S. “Nucleation of Sodium
651 Sulfate Heptahydrate on Mineral Substrates Studied by Nuclear Magnetic Resonance.”
652 Journal of Crystal Growth 338, no. 1 (2012): 166–169.
653 [20] Denecker, M. F. C., Hebert, R. L., Wassermann, . J. , Dosseh, G. , Menendez, B. and
654 Bourgès, A. “Experimental Study of the Crystallization of Sodium Sulfate Hydrates
655 through Temperature Monitoring.” Environmental Earth Sciences 72, no. 12 (2014):
656 5089–5099.
657 [21] Steiger, M., and Asmussen, S. “Crystallization of Sodium Sulfate Phases in Porous
658 Materials: The Phase Diagram Na 2 SO 4–H 2 O and the Generation of Stress.”
659 Geochimica et Cosmochimica Acta 72, no. 17 (2008): 4291–4306.
660 [22] Genkinger, S. and Putnis, A., 2007. Crystallisation of sodium sulfate: supersaturation and
661 metastable phases. Environmental geology, 52(2), pp.329-337.
662 [23] Espinosa, R. M., Franke, L., and Deckelmann, G. “Phase Changes of Salts in Porous
663 Materials: Crystallization, Hydration and Deliquescence.” Construction and Building
664 Materials 22, no. 8 (2008): 1758–1773.
665 [24] Desarnaud, J., and Shahidzadeh-Bonn, N. “Salt Crystal Purification by
666 Deliquescence/crystallization Cycling.” EPL (Europhysics Letters) 95, no. 4 (2011):
667 48002.
668 [25] Shahidzadeh-Bonn, N., Rafaı, S., Bonn, D., and Wegdam, G. “Salt Crystallization during
669 Evaporation: Impact of Interfacial Properties.” Langmuir 24, no. 16 (2008): 8599–8605.
670 [26] López-Arce, P., and Doehne, E. “Kinetics of Sodium Sulfate Efflorecence as Observed by
671 Humidity Cycling with ESEM.” In Proceed. Int. Conf. on Heritage, Weathering and
672 Conservation, 285–291, 2006.

673 [27] Linnow K., Zeunert, A.and Steiger, M. “Investigation of sodium sulfate phase transitions
674 in a porous material using humidity- and temperature-controlled x-ray diffraction” .
675 Anal. Chem. 78, (2006) 4683-4689.
676 [28] Hamilton, A., and Menzies, R.I. “Raman Spectra of Mirabilite, Na2SO4· 10H2O and the
677 Rediscovered Metastable Heptahydrate, Na2SO4· 7H2O.” Journal of Raman
678 Spectroscopy 41, no. 9 (2010): 1014–1020.
679 [29] Linnow, K., Steiger, M., Lemster, C., De Clercq, H.,and Jovanović, M. “In Situ Raman
680 Observation of the Crystallization in NaNO3–Na2SO4–H2O Solution Droplets.”
681 Environmental Earth Sciences 69, no. 5 (2013): 1609–1620.
682 [30] Derluyn, H., Dewanckele, J., Boone, M.N., Cnudde, V., Derome, D. and Carmeliet, J.,
683 2014. Crystallization of hydrated and anhydrous salts in porous limestone resolved by
684 synchrotron X-ray microtomography. Nuclear Instruments and Methods in Physics
685 Research Section B: Beam Interactions with Materials and Atoms, 324, pp.102-112.
686 [] Egan, T., Rodriguez-Pascual, M. and Lewis, A. “In Situ Growth Measurements of Sodium
687 Sulfate during Cooling Crystallization.” Chemical Engineering & Technology 37, no. 8
688 (2014): 1283–1290.
689 [32] Benavente, D., del Cura, M.G., Fort, R. and Ordóñez, S., 1999. Thermodynamic modelling
690 of changes induced by salt pressure crystallisation in porous media of stone. Journal of
691 Crystal growth, 204(1), pp.168-178.
692 [33] Benavente, D., Brimblecombe, P. and Grossi C.M. (2015), Thermodynamic calculations
693 for the salt crystallisation damage in porous built heritage using PHREEQC.
694 Environmental Earth Sciences 74 (3), 2297-2313
695 [34] Chauvet, F., Cazin, S., Duru, P. and Prat, M., 2010. Use of infrared thermography for the
696 study of evaporation in a square capillary tube. International Journal of Heat and Mass
697 Transfer, 53(9), pp.1808-1818.
698 [35] Bagavathiappan, S., Lahiri, B. B., Saravanan, T. John Philip, and Jayakumar, T. “Infrared

699 Thermography for Condition Monitoring–a Review." Infrared Physics & Technology 60
700 (2013): 35–55.
701 [36] Grinzato, E., Vavilov, V. and Kauppinen. T. "Quantitative Infrared Thermography in
702 Buildings." Energy and Buildings 29, no. 1 (1998): 1–9.
703 [37] Grinzato, E., Bison, P. G. and Marinetti S. "Monitoring of Ancient Buildings by the Thermal
704 Method." Journal of Cultural Heritage 3, no. 1 (2002): 21–29.
705 [38] Avdelidis, N.P. and Moropoulou, A., 2003. "Emissivity considerations in building
706 thermography". Energy and Buildings, 35(7), pp.663-667.
707 [39] Avdelidis, N.P. and Moropoulou, A., 2004. "Applications of infrared thermography for the
708 investigation of historic structures". Journal of Cultural Heritage, 5(1), pp.119-127.
709 [40] Bodnar, J.L., Mouhoubi, K., Di Pallo, L., Detalle, V., Vallet, J.M. and Duvaut, T., 2013.
710 "Contribution to the improvement of heritage mural painting non-destructive testing by
711 stimulated infrared thermography". The European Physical Journal Applied
712 Physics, 64(1), p.11002.
713 [41] Thomachot-Schneider, C., Vazquez, P., Lelarge, N., Bouvy, C., Gommeaux, M., Mouhoubi,
714 K. and Bodnar, J.L., 2014. "Thermal behaviour of building stones submitted to salt
715 solutions". In *SWBSS 3rd International Conference on Salt Weathering of Buildings and*
716 *Stone Sculptures, Brussels*.
717 [42] Thomachot-Schneider, C., Gommeaux, M., Lelarge, N., Conreux, A., Mouhoubi, K.,
718 Bodnar, J.L. and Vázquez, P., 2016. "Relationship between Na2SO4 concentration and
719 thermal response of reconstituted stone in the laboratory and on site". Environmental
720 Earth Sciences, 75(9), pp.1-12.
721 [43] Mouhoubi, K. Bodnar, J-L ., Vallet, J.M., Detalle, V., Vázquez, P. , Thomachot-Schneider
722 C. 2016. "Detection of NaCl located in mural painting by stimulated infrared
723 thermography", QIRT 2016, Gdansk (Pologne)
724 [44] Parsa, M., Harmand, S., Sefiane, K., Bigerelle, M., and Deltombe R. "Effect of Substrate

725 Temperature on Pattern Formation of Nanoparticles from Volatile Drops." Langmuir 31,
726 no. 11 (2015): 3354–3367.
727 [45] Vázquez, P., Thomachot-Schneider, C., Mouhoubi, K., Fronteau, G., Gommeaux, M.,
728 Benavente, D., Barbin, V., and Bodnar, J.L. "Infrared Thermography Monitoring of the
729 NaCl Crystallisation Process." Infrared Physics & Technology 71 (2015): 198–207.
730 [46] Vázquez, P., Thomachot-Schneider, C., Mouhoubi, K., Gommeaux, M., Fronteau, G.,
731 Barbin, V. and Bodnar, J.L., 2014, October. "Study of NaCl crystallization using infrared
732 thermography". In *SWBSS 3rd International Conference on Salt Weathering of*
733 *Buildings and Stone Sculptures, Brussels*.
734 [47] FLIR user manual. Series SC 655.
735 [48] Gaussorgues, G. "La thermographie infrarouge: principes-techniques–applications,
736 Quatrième édition revue et argumentée." (1999): 2-7430.
737 [49] Saidov, T. A., Shahidzadeh, N., and Pel, L. "Crystallization of Sodium Sulfate on
738 Hydrophilic/hydrophobic Surfaces during Drying: An NMR Study." EPL (Europhysics
739 Letters) 102, no. 2 (2013): 28003.
740 [50] Vavouraki, A. I., and Koutsoukos P. G. "Kinetics of Crystal Growth of Mirabilite in Aqueous
741 Supersaturated Solutions." Journal of Crystal Growth 338, no. 1 (2012): 189–194.
742 [51] Roy, B., Dutta Choudhuri, M., Dutta, T.,and Tarafdar S., "Multi-Scale Patterns Formed by
743 Sodium Sulfate in a Drying Droplet of Gelatin." Applied Surface Science 357 (2015):
744 1000–1006.
745 [52] Mullin, J. W. *Crystallization*. Butterworth-Heinemann. (2001).
746 [53] Saidov, T. A., Pel, L. and van der Heijden G. H. A. "Crystallization of Sodium Sulfate in
747 Porous Media by Drying at a Constant Temperature." International Journal of Heat and
748 Mass Transfer 83 (2015): 621–628.
749 [54] Hird, R., and M. D. Bolton. "Measurement of Relative Humidity to Monitor Salt Migration in
750 Unsaturated Porous Media." Transport in Porous Media 112, no. 3 (2016): 749–763.

751 [55] Füredi-Milhofer, H., Babić-Ivančić V., Brečević L., Filipović-Vinceković, N., Kralj, D.,
752 Komunjer, L., Marković, M. and Drago Škrtić. “Factors Influencing Nucleation from
753 Solutions Supersaturated to Different Crystal Hydrates.” Colloids and Surfaces 48
754 (1990): 219–230.
755
756

Conflict of interest

The authors declare that there is no conflict of interest with this work.